



NIST
PUBLICATIONS

Applied and
Computational
Mathematics
Division

NISTIR 4971

Computing and Applied Mathematics Laboratory

*Asymptotic Behavior of Modulated
Taylor-Couette Flows with a Crystalline
Inner Cylinder*

*R. J. Braun, G. B. McFadden, B. T. Murray,
S. R. Coriell, M. E. Glicksman,
and M. E. Selleck*

November 1992

Technology Administration
U.S. DEPARTMENT OF COMMERCE
National Institute of Standards and Technology
Gaithersburg, MD 20899

QC
100
.U56
4971
1992

NIST IR

NISTIR 4971

QC
100
.456
4971
1992

Asymptotic Behavior of Modulated Taylor-Couette Flows with a Crystalline Inner Cylinder

**R. J. Braun
G. B. McFadden
B. T. Murray
S. R. Coriell
M. E. Glicksman
M. E. Selleck**

U.S. DEPARTMENT OF COMMERCE
Technology Administration
National Institute of Standards
and Technology
Applied and Computational Mathematics Division
Computing and Applied Mathematics Laboratory
Gaithersburg, MD 20899

November 1992



**U.S. DEPARTMENT OF COMMERCE
Barbara Hackman Franklin, Secretary**

**TECHNOLOGY ADMINISTRATION
Robert M. White, Under Secretary for Technology**

**NATIONAL INSTITUTE OF STANDARDS
AND TECHNOLOGY
John W. Lyons, Director**

NIST IR
QC
100
.456
4471
1992

Asymptotic Behavior of Modulated Taylor-Couette Flows with a Crystalline Inner Cylinder

R. J. Braun, G. B. McFadden, B. T. Murray, and S. R. Coriell
National Institute of Standards and Technology*
Gaithersburg, MD 20899

and

M. E. Glicksman and M. E. Selleck
Department of Materials Engineering
Rensselaer Polytechnic Institute
Troy, NY 12181

November 4, 1992

Abstract

We consider the linear stability of a modulated Taylor-Couette system when the inner cylindrical boundary consists of a crystalline solid-liquid interface. Both experimentally and in numerical calculations it is found that the two-phase system is significantly less stable than the analogous rigid-walled system for materials with moderately large Prandtl numbers. A numerical treatment based on Floquet theory is described, which gives results that are in good agreement with preliminary experimental findings. In addition, this instability is further examined by carrying out a formal asymptotic expansion of the solution in the limit of large Prandtl number. In this limit the Floquet analysis is considerably simplified, and the linear stability of the modulated system can be determined to leading order through a conventional stability analysis, without recourse to Floquet theory. The resulting simplified problem is then studied for both the narrow gap geometry and for the case of a finite gap. It is surprising that the determination of the linear stability of the two-phase system is considerably simpler than that of the rigid-walled system, despite the complications introduced by the presence of the crystal-melt interface. PACS: 47.30.+s, 47.20.-k, 81.10.Fq, 81.30.Fb

*Technology Administration, U.S. Department of Commerce, Washington, D.C.

1. Introduction

An important consideration in the growth of multicomponent single crystals from the melt is the spatial distribution of solute. In many instances, inhomogeneities in the solute distribution result in inferior electrical and mechanical properties. It is therefore desirable to understand the physical mechanisms that lead to solute segregation in melt-grown crystals.

Since solid state diffusion normally occurs at rates several orders of magnitude lower than in the melt phase, the distribution of solute in the crystal is primarily determined by the solute profile in the liquid immediately ahead of the advancing crystal-melt interface; as the liquid transforms into solid, little rearrangement of the solute distribution takes place. Thus the prediction of the solute distribution in the crystal requires the understanding of solute transport in the melt adjacent to the crystal-melt interface [1, 2]; in particular, mechanisms that produce lateral segregation of solute along the interface play a major role.

During directional solidification (see, e.g., [3]) under ideal processing conditions, a planar crystal-melt interface advances at constant velocity into a quiescent melt, in which case the crystal that is produced is spatially homogeneous. Loss of ideality can arise in many ways; two of the more extensively studied mechanisms are *morphological instability* of the crystal-melt interface [4, 5], which causes a planar crystal-melt to develop a corrugated lateral structure with accompanying solute redistribution, and *hydrodynamic instabilities* in the melt [6, 7, 8], in which solute inhomogeneities are associated with the features of the secondary flow fields.

Although these two mechanisms can be studied separately, it is important to understand how the two are related. Hydrodynamic flows occur frequently during crystal growth from the melt, either naturally or by design. It is desirable to be able to predict whether a particular flow will generate a strong coupling with the crystal-melt interface, possibly enhancing morphological instability. It is similarly important to know whether the presence of the crystal-melt interface will cause significant changes in the hydrody-

dynamic instabilities that occur in classical, fixed-boundary systems. If the flow/interface interaction is particularly strong, of course, then the classification of the underlying instability as being either morphological or hydrodynamic in nature may be overly simplistic.

A number of authors have considered the morphological stability of the crystal-melt interface in the presence of various types of flow fields. Examples include plane Couette flow [9, 10], thermosolutal convection [11, 12], plane stagnation flow [13, 14], rotating disk flow [15], and the asymptotic suction profile [16]. The effect of a crystal-melt interface on the hydrodynamic stability of the melt has also been considered for a variety of flows, including Rayleigh-Bénard convection [17], thermosolutal convection [7, 18, 19], plane Poiseuille flow [20], the asymptotic suction profile [16], thermally-driven flow in an annulus [21, 20], and steady Taylor-Couette flow [22, 23].

Particularly strong flow/interface interactions were observed in two of these cases. For flow in a vertical annulus with radial heating, with the outer annular boundary consisting of a cylindrical crystal-melt interface, Fang et al. [21, 20] found that the two-phase system is destabilized by an order of magnitude compared to the rigid-walled system. The material studied was succinonitrile (SCN), which has a moderately large Prandtl number of about 23. In the rigid-walled system, the most dangerous mode under these conditions is an axisymmetric buoyant instability. The most dangerous mode for the two-phase system is given by a non-axisymmetric, helical instability which ensues at much lower radial temperature differences; moreover, this mode appears as a destabilization of a shear mode which, in the rigid-walled system, is considerably more stable than the buoyant mode. Numerical parameter studies of the linear stability of the two-phase system show that the helical instability is dominant for crystals with melts that have large Prandtl numbers. In steady Taylor-Couette flow [24], another strong coupling occurs if one of the cylindrical boundaries again consists of the crystalline phase of the melt contained in the annular region [22, 23]; this effect is also found to provide significant destabilization of the flow for melts with high Prandtl numbers.

In this paper we consider an unsteady version of the Taylor-Couette experiment, in

which strong destabilization of the hydrodynamic instability is observed for the two-phase system. We consider the linear stability of a Taylor-Couette geometry in which the entire system undergoes a torsional oscillation about the cylindrical axis. Preliminary experiments for this problem have been performed using SCN, and show a marked destabilization of the system over a range of frequencies [25]. Numerical studies have also been performed using Floquet theory to describe the linear stability of the system; the numerical results show similar behavior with qualitative agreement between the theory and the preliminary experiments. Since the strong flow/interface coupling is found to be most significant for moderately large Prandtl numbers, we examine here the asymptotic limit $Pr \gg 1$. Somewhat surprisingly, we find that in this limit we are able to obtain a quite tractable description of the linear stability of the two-phases system without recourse to Floquet theory. The strong destabilization provided by the crystal-melt interface for $Pr \gg 1$ actually results in a much simpler analysis for the two-phase system than that obtained for the single-phase system with rigid walls [26, 27].

In the following section we describe briefly preliminary experiments which have been performed for this problem. This is followed by a description of a numerical treatment of the linear stability problem based on a pseudospectral spatial discretization of the linearized governing equations with a Floquet analysis in the time variable. The approach is described both in the simpler narrow gap limit of the governing equations [28], and for the more general case of a finite gap. The asymptotic analysis for large Prandtl number is described for both the narrow and finite gap, and the numerical and asymptotic results are compared with the experimental results. Some remarks concerning the relevance of the findings to the more general problem of predicting the strength of flow/interface interaction are given in the conclusion.

2. Modulated Taylor-Couette Flow

The experiment is performed using succinonitrile; the relevant material properties are given in Ref. [21]. The apparatus consists of two coaxial cylinders which are sealed

together at both ends to provide a single, rigid unit; the succinonitrile occupies the space between the cylinders. A radial temperature difference is maintained across the sample by circulating a cooling fluid with temperature T_0 inside the inner cylinder, while the whole apparatus is situated in a bath held at a uniform temperature $T_2 > T_0$. If these temperatures are chosen on either side of the melting point T_M of SCN, so that $T_0 < T_M < T_2$, then a cylindrical crystal-melt interface forms at an intermediate radius R_1 . A schematic diagram with a corrugated crystal-melt interface is shown in Figure 1. To produce a modulated Taylor-Couette flow, the entire apparatus is oscillated about the cylindrical axis of the system. Accurate control of the oscillation was devised by using a mechanical linkage to the servo-motor of a chart recorder to drive the system, with the input to the chart recorder provided by a signal generator to allow a wide variation in the waveform and frequency of the modulation.

The outer diameter of the smaller cylinder is 1.2 cm, and the inner diameter of the larger cylinder is 3.3 cm. The length of the straight portion of the apparatus is 24.1 cm, with a further 2 cm of tapering on each end where the walls are joined together. The choice to perform the rigid-body rotation of the coaxial cylinders without differential rotation was made to avoid complications with seals that allow slip at the endwalls. The design of the drive allows variation in both the frequency and amplitude of the torsional oscillation of the system. In the preliminary experiments performed thus far, the stability boundaries were determined by fixing the frequency and varying the amplitude of the oscillation, using a pure sinusoidal waveform from the signal generator. Oscillation frequencies up to a few Hertz can be produced reliably with this design.

In a typical experimental run, a crystal-melt interface is established within the glass-walled annulus by maintaining a temperature difference of a few degrees Kelvin across the gap, with the mean temperature near the melting point. For small amplitudes of modulation, the interface is cylindrical in shape except near the tapered endwalls of the container. At larger amplitudes, the interface is observed to develop well-defined oscillations along the axial direction. The resulting deformation of the interface appears

axisymmetric, and the amplitude of the interface deformation appears steady in time. By performing a series of runs, stability limits for the modulation amplitude associated with the breakdown of the cylindrical crystal-melt interface could be determined as a function of the oscillation frequency. As described below, the two-phase system is found to become unstable at amplitudes that are an order of magnitude lower than those required for the instability of the analogous single-phase, rigid-walled coaxial system.

Rudimentary flow visualization is possible by using a video camera to provide images of the system from a side view. By examining the motion of a particle in the melt, it is possible to determine the nature of the flow field associated with the instability of the crystal-melt interface. At a given instant of time, the flow consists of Taylor vortices stacked along the apparatus in the axial direction, with the wavelength of the interface deformation given by the extent of a pair of the counter-rotating cells. In Figure 2 we show a multiple exposure photograph that shows the motion of an irregularly-shaped particle in a single cell. The multiple exposure was taken in two steps. First, a continuous recording of the video tape was edited to give a sequence of individual frames that are each separated in time by one period of the oscillation frequency. In the resulting film the particle is observed to circulate along a closed path in the same azimuthal plane. The multiple exposure photo was then assembled from several of these frames to illustrate the path of the particle; the positions of the particle in Figure 2, however, are not sequential, and were chosen to give a rough indication of the particle trajectory.

The particle moves radially inward from the hot outer cylinder towards the minimum in the interface deformation (largest liquid gap), where hot fluid flows towards the crystal-melt interface, and returns toward the outer cylinder near the maximum in the interface deformation. The deformation is consistent with the average temperature of the fluid, since the heating provided by the outer cylinder relative to the relatively-cooler crystal-melt interface implies that the interface melts back under the impingement of warmer fluid, and bulges out under the influence of the cooler fluid. The wavelength of the Taylor vortices is significantly longer than that observed for the single-phase system; quantitative

comparisons will be provided below, together with the discussion of theoretical results.

3. Theory

The determination of linear stability for rigid-walled systems undergoing modulated oscillations has been performed by a number of authors, including Riley and Lawrence [29], Carmi and Tustaniwskyj [30], Barenghi and Jones [31], Kuhlmann et al. [32], Wu and Swift [33], and Murray et al. [34]. Here we consider the pure torsional oscillation of a Taylor-Couette apparatus for the case of a two-phase system with a crystal-melt interface providing one of the bounding surfaces of the flow. The analysis assumes an axisymmetric geometry, which is consistent with the experimental observations for the two-phase system. Both narrow and wide gap formulations are considered. For simplicity, gravity-induced buoyancy effects and similar effects related to the radial density stratification are ignored; these effects were considered for the unmodulated case in Ref. [35], and were found to provide only minor corrections to the stability results.

3.1. Wide Gap

The rigid-body torsional oscillation for sufficiently large angular speeds will produce a centrifugal instability in the base flow [26, 27]. As depicted in Figure 1, we employ a cylindrical coordinate system (r', ϕ', z') , and consider the linear stability of an idealized base state that extends to infinity in the axial direction (primed quantities will be dimensional). The rigid inner wall is at $r' = R_0$, and the outer rigid wall is at $r' = R_2$. The axisymmetric crystal-melt interface is given by $r' = R_1(z', t')$; in the base state the interface is cylindrical, with a constant radius $R_1(z', t') = \bar{R}_1$. The gap $R_1(z', t') < r' < R_2$ contains the incompressible melt or liquid phase, and the crystal or solid phase occupies the remainder of the domain. The entire apparatus is oscillated torsionally, so that at the undisturbed crystal-melt interface the azimuthal velocity is given by $v' = \bar{R}_1 \Omega_1(t)$, and at the outer wall, $v' = R_2 \Omega_1(t)$; here $\Omega_1(t) = \Omega \cos(\omega' t')$ and Ω is the amplitude of the oscillations. The radial and axial velocities at the melt boundaries are given by

$u' = w' = 0$, respectively. In the gap, the melt velocity is divergence-free and satisfies the Navier-Stokes equations in cylindrical coordinates. We assume that the flow is axisymmetric, as observed in the experiment. We scale the radial and axial velocities with ν/L where $L = R_2 - \bar{R}_1$ is the gap width, and ν is the kinematic viscosity, and scale the azimuthal velocity with $\bar{R}_1\Omega$. We scale the spatial coordinates as $r' = Lr$, $z' = Lz$, scale the time as $\omega't' = \tau$, and scale the pressure as $\rho\nu^2/L^2$. The deviations of the temperature fields in the melt and solid from the equilibrium value established by the crystal-melt interface are scaled with the temperature difference ΔT across the gap, for example,

$$T_L = \frac{T'_L - T_M(1 - \Gamma/\bar{R}_1)}{\Delta T}, \quad (1)$$

where

$$\Delta T = T_2 - T_M(1 - \Gamma/\bar{R}_1), \quad (2)$$

and Γ is a capillary constant related to the depression of the melting point by interface curvature (the Gibbs-Thomson effect). The crystal-melt interface (at \bar{R}_1 in the base state) is located at

$$r' = \bar{R}_1 + Lh(z, t) \quad (3)$$

when disturbed. In dimensionless form, the domain is $r_0 \leq r \leq r_2$, where $r_0 = \eta_S/(1 - \eta)$ and $r_2 = 1/(1 - \eta)$, with $\eta = \bar{R}_1/R_2$ and $\eta_S = R_0/R_2$. The melt occupies the region $r_1 + h(z, t) < r < r_2$, where $r_1 = \eta/(1 - \eta)$. In the linearized theory, the disturbance of the crystal-melt interface location h will be taken close to zero, and the interfacial conditions will be referred to r_1 in the usual way. Neglecting all derivatives in the azimuthal direction, we obtain the governing equations on $r_1 \leq r \leq r_2$,

$$\frac{\partial u}{\partial r} + \frac{\partial w}{\partial z} = 0, \quad (4)$$

$$\omega \frac{\partial u}{\partial \tau} + u \frac{\partial u}{\partial r} + w \frac{\partial u}{\partial z} - \frac{\eta}{2(1 - \eta)} \text{Ta} \frac{v^2}{r} = -\frac{\partial p}{\partial r} + \frac{\partial u}{\partial r^2} + \frac{1}{r} \frac{\partial u}{\partial r} - \frac{u}{r^2} + \frac{\partial^2 u}{\partial z^2}, \quad (5)$$

$$\omega \frac{\partial v}{\partial \tau} + u \frac{\partial v}{\partial r} + w \frac{\partial v}{\partial z} + \frac{uv}{r} = \frac{\partial v}{\partial r^2} + \frac{1}{r} \frac{\partial v}{\partial r} - \frac{v}{r^2} + \frac{\partial^2 v}{\partial z^2}, \quad (6)$$

$$\omega \frac{\partial w}{\partial \tau} + u \frac{\partial w}{\partial r} + w \frac{\partial w}{\partial z} = -\frac{\partial p}{\partial z} + \frac{\partial w}{\partial r^2} + \frac{1}{r} \frac{\partial w}{\partial r} + \frac{\partial^2 w}{\partial z^2}, \quad (7)$$

where the Taylor number is given by $Ta = 2\bar{R}_1\Omega^2L^3/\nu^2$, and $\omega = \omega'L^2/\nu$; here ν is the kinematic viscosity of the melt. In addition to the equations of fluid motion, there will be energy equations in the melt and solid. In the melt,

$$\omega \frac{\partial T_L}{\partial \tau} + u \frac{\partial T_L}{\partial r} + w \frac{\partial T_L}{\partial z} = \frac{1}{Pr} \left(\frac{\partial T_L}{\partial r^2} + \frac{1}{r} \frac{\partial T_L}{\partial r} + \frac{\partial^2 T_L}{\partial z^2} \right), \quad (8)$$

and in the solid

$$\omega \frac{\partial T_S}{\partial \tau} = \frac{1}{Ps} \left(\frac{\partial T_S}{\partial r^2} + \frac{1}{r} \frac{\partial T_S}{\partial r} + \frac{\partial^2 T_S}{\partial z^2} \right), \quad (9)$$

where $Pr = \nu/\kappa_L$ is the Prandtl number of the melt, and $Ps = \nu/\kappa_S$; here κ_L, κ_S are the thermal diffusivities of the liquid and solid phases respectively.

The solid temperature is prescribed on the inner rigid wall, $r = r_0$, and on the outer rigid wall, $r = r_2$, we have

$$u = w = 0, \quad T_L = 1, \quad v = (1/\eta) \cos \tau. \quad (10)$$

On the interface $r = \eta/(1 - \eta) + h$, we have

$$u = w = 0, \quad (11)$$

$$v = \left(1 + \frac{1 - \eta}{\eta} h \right) \cos \tau, \quad (12)$$

$$T_L = T_S = \gamma \mathcal{K}, \quad (13)$$

and

$$-\mathcal{L}\omega \frac{\partial h}{\partial \tau} = \frac{\partial T_L}{\partial r} - \frac{\partial h}{\partial z} \frac{\partial T_L}{\partial z} - q \left(\frac{\partial T_S}{\partial r} - \frac{\partial h}{\partial z} \frac{\partial T_S}{\partial z} \right). \quad (14)$$

Here \mathcal{K} is twice the mean curvature in cylindrical coordinates, $\gamma = T_M\Gamma/(L\Delta T)$ is proportional to the surface energy, $q = k_S/k_L$ is the ratio of the thermal conductivities in the crystal and the melt respectively, and $\mathcal{L} = \nu L_v/(k_L\Delta T)$ is proportional to the latent heat L_v released upon solidification.

The Taylor number may be related to the Reynolds number Re used in previous work [25] by

$$Ta = \frac{2\eta}{1 - \eta} Re^2, \quad (15)$$

where $\text{Re} = \Omega L^2 / \nu$. This definition of the Taylor number is identical to that used by Hall *et al* [26, 27].

3.1.1. Base State

We seek a base state that is only dependent on r and t . The base state flow field is given by $u^{(0)} = w^{(0)} = 0$ and $v^{(0)} = \text{Real}[V_0(r)e^{i\tau}]$, and where $V_0(r)$ satisfies

$$\frac{\partial V_0}{\partial r^2} + \frac{1}{r} \frac{\partial V_0}{\partial r} - \left(\frac{1}{r^2} + i\omega \right) V_0 = 0, \quad (16)$$

subject to $V_0(r_1) = 1$ and $V_0(r_2) = 1/\eta$. Though the solution may be written in terms of Kelvin functions, we choose to integrate it numerically at the collocation points used in the subsequent discretization. The thermal fields satisfy ordinary differential equations in r ; the time-independent base states for the temperature fields are given by

$$T_L^{(0)} = -\frac{\ln[r(1-\eta)/\eta]}{\ln \eta}, \quad (17)$$

and

$$T_S^{(0)} = -\frac{\ln[r(1-\eta)/\eta]}{q \ln \eta}. \quad (18)$$

The base state interface shape is given by $h^{(0)} = 0$. The base state pressure gradient may be determined from the radial momentum equation.

3.1.2. Linearized Equations

We perturb the base state and denote the disturbance quantities by a superscript (1).

Assuming normal-mode, small-amplitude disturbances, we write

$$\begin{pmatrix} u \\ v \\ w \\ p \\ T_L \\ T_S \\ h \end{pmatrix} = \begin{pmatrix} 0 \\ v^{(0)}(r, \tau) \\ 0 \\ p^{(0)}(r, \tau) \\ T_L^{(0)}(r) \\ T_S^{(0)}(r) \\ 0 \end{pmatrix} + \begin{pmatrix} u^{(1)}(r, \tau) \\ v^{(1)}(r, \tau) \\ w^{(1)}(r, \tau) \\ p^{(1)}(r, \tau) \\ T_L^{(1)}(r, \tau) \\ T_S^{(1)}(r, \tau) \\ h^{(1)}(\tau) \end{pmatrix} \exp(iaz), \quad (19)$$

where a is the axial wavenumber. Eliminating the pressure $p^{(1)}$ and axial velocity $w^{(1)}$, the linearized equations become

$$\omega (DD_* - a^2) \frac{\partial u^{(1)}}{\partial \tau} + a^2 \frac{\eta}{(1-\eta)} \text{Ta} \frac{v^{(0)}}{r} v^{(1)} = (D^2 D_*^2 - 2a^2 DD_* + a^4) u^{(1)}, \quad (20)$$

$$\omega \frac{\partial v^{(1)}}{\partial \tau} + (D_* v^{(0)}) u^{(1)} = (DD_* - a^2) v^{(1)}, \quad (21)$$

$$\omega \frac{\partial T_L^{(1)}}{\partial \tau} + D(T_L^{(0)}) u^{(1)} = \frac{1}{\text{Pr}} (D_* D - a^2) T_L^{(1)}, \quad (22)$$

on $r_1 \leq r \leq r_2$, and in the solid $r_0 \leq r \leq r_1$,

$$\omega \frac{\partial T_S^{(1)}}{\partial \tau} = \frac{1}{\text{Ps}} (D_* D - a^2) T_S^{(1)}. \quad (23)$$

Here $D = \partial/\partial r$ and $D_* = \partial/\partial r + 1/r$.

At the inner solid wall $r_0 = \eta_S/(1-\eta)$, we set $T_S^{(1)} = 0$, and at the outer wall $r = r_2 = 1/(1-\eta)$, we require

$$v^{(1)} = u^{(1)} = Du^{(1)} = T_L^{(1)} = 0. \quad (24)$$

At $r = r_1 = \eta/(1-\eta)$ the crystal-melt interface boundary conditions are

$$u^{(1)} = Du^{(1)} = 0, \quad (25)$$

$$v^{(1)} + \left(-\frac{1-\eta}{\eta} \cos \tau + Dv^{(0)} \right) h^{(1)} = 0, \quad (26)$$

$$\mathcal{L}\omega \frac{\partial h^{(1)}}{\partial \tau} + DT_L^{(1)} - qDT_S^{(1)} = 0, \quad (27)$$

$$T_L^{(1)} + (DT_L^{(0)})h^{(1)} = T_S^{(1)} + (DT_S^{(0)})h^{(1)}/q = \gamma (1/r_1^2 - a^2) h^{(1)}. \quad (28)$$

The above set of equations have temporally-periodic coefficients that vary spatially as well; the solutions may be determined from an application of Floquet theory.

3.2. Narrow Gap

3.2.1. Scalings and Base State

We shall also study the simplified system of equations that results in the narrow gap limit. All scales remain the same except that we now scale the radial coordinate as $r' = R_1 + Lx$; in nondimensional form, $r = r_1 + x$. The melt/solid interface that is at $r_1 = \eta/(1 - \eta)$ in the base state will be located at

$$r = r_1 + h, \quad (29)$$

where the nondimensional interface amplitude h is scaled with the gap width. In nondimensional form, the domain becomes $x_0 \leq x \leq 1$, where

$$x_0 = (\eta_S - \eta)/(1 - \eta) \quad (30)$$

with the melt occupying $h < x < 1$. In the linearized theory, the melt/solid interface location h will be taken close to zero.

In this limit, we assume $1 - \eta = \varepsilon \ll 1$, and that the Taylor number and the dependent variables remain $O(1)$. We then have $T_L^{(0)} = x + O(\varepsilon)$, $T_S^{(0)} = x/q + O(\varepsilon)$, and the base state velocity profile now satisfies $u^{(0)} = w^{(0)} = 0$ and

$$\omega v_\tau^{(0)} = v_{xx}^{(0)}, \quad v^{(0)}(0, \tau) = v^{(0)}(1, \tau) = \cos \tau \quad (31)$$

The solution for the azimuthal component is

$$v^{(0)} = \text{Real} \left\{ e^{i\tau} \frac{\cosh \left[\sqrt{i\omega} (x - 1/2) \right]}{\cosh(\sqrt{i\omega}/2)} \right\}. \quad (32)$$

The pressure $p^{(0)}$ may be again determined from the radial momentum equation.

3.2.2. Linearized Equations

We may disturb the basic state as in Eq. (19), and eliminating the pressure $p^{(1)}$ and axial velocity $w^{(1)}$, the linearized equations become

$$\omega \left(\frac{\partial^2}{\partial x^2} - a^2 \right) \frac{\partial u^{(1)}}{\partial \tau} + a^2 \text{Ta} v^{(0)} v^{(1)} = \left(\frac{\partial^2}{\partial x^2} - a^2 \right)^2 u^{(1)}, \quad (33)$$

$$\omega \frac{\partial v^{(1)}}{\partial \tau} + \frac{\partial v^{(0)}}{\partial x} u^{(1)} = \left(\frac{\partial^2}{\partial x^2} - a^2 \right) v^{(1)}, \quad (34)$$

$$\omega \frac{\partial T_L^{(1)}}{\partial \tau} + u^{(1)} = \frac{1}{\text{Pr}} \left(\frac{\partial^2}{\partial x^2} - a^2 \right) T_L^{(1)}, \quad (35)$$

on $0 \leq x \leq 1$, and in the solid $x_0 \leq x \leq 0$,

$$\omega \frac{\partial T_S^{(1)}}{\partial \tau} = \frac{1}{\text{Ps}} \left(\frac{\partial^2}{\partial x^2} - a^2 \right) T_S^{(1)}. \quad (36)$$

At the inner solid wall $x_0 = (\eta_S - \eta)/(1 - \eta)$,

$$T_S^{(1)} = 0. \quad (37)$$

At the outer wall $x = 1$,

$$v^{(1)} = u^{(1)} = \frac{\partial u^{(1)}}{\partial x} = T_L^{(1)} = 0. \quad (38)$$

At the crystal-melt interface referred to $x = 0$,

$$u^{(1)} = \frac{\partial u^{(1)}}{\partial x} = 0, \quad (39)$$

$$v^{(1)} + \frac{\partial v^{(0)}}{\partial x} h^{(1)} = 0, \quad (40)$$

$$-\mathcal{L}\omega \frac{\partial h^{(1)}}{\partial \tau} = \frac{\partial T_L^{(1)}}{\partial x} - q \frac{\partial T_S^{(1)}}{\partial x}, \quad (41)$$

$$T_L^{(1)} + h^{(1)} = T_S^{(1)} + \frac{1}{q} h^{(1)} = -\gamma a^2 h^{(1)}. \quad (42)$$

Because of the spatial and temporal variation in $v^{(0)}(r, t)$ we must solve this problem numerically for most values of the parameters.

4. Numerical Formulations

In general, the above set of equations must be solved numerically. We have carried out a pseudospectral discretization in the spatial variable r ; the resulting system of ordinary differential equations subject to algebraic constraints may be integrated over one period in time, and the Floquet exponents computed; we may then determine the stability of the base state. We may also Fourier expand the solutions in time and find the growth rate of each mode by solving the resulting two-point boundary value problems as described elsewhere[25]. We have employed both procedures as a check on our numerics.

4.1. Wide Gap

We discretize the derivatives in the radial direction using the standard Chebyshev pseudospectral method (see, e.g., [37, 38]). It is convenient for this method to rescale the radial variable. In the liquid we set $r = r_1 + \frac{1}{2}(\xi + 1)$ for $-1 < \xi < 1$, and in the solid we set $r = r_0 + \frac{1}{2}(\xi + 1)x_0$. Then in the liquid we have $d/dr = 2d/d\xi$ and in the solid we have $d/dr = -(2/x_0)d/d\xi$.

We use the points $\xi_j = \cos j\pi/n$ for $j = 0, 1, \dots, n$, so that the interface is located at $\xi_0 = 1$. At the collocation points we use the Chebyshev derivative matrix D [38], which has the property that at the collocation points ξ_j the derivative g'_j of an n -th degree polynomial $g(\xi)$ is given exactly in terms of its collocation values g_k by the expression

$$g'_j = \sum_{k=0}^n D_{jk} g_k. \quad (43)$$

Higher derivatives are represented by powers D^m of the matrix D . We write $g'_j = D_{jk} g_k$ and thereby let the sum over the repeated index k be implied. D_{ij} is the differentiation matrix in the melt, and \hat{D}_{ij} is the differentiation matrix in the solid.

For convenience, we drop the superscript on the disturbance quantities; at the interior points in the melt ξ_j , $j = 1, \dots, n-1$, we have the discretized equations

$$\omega \frac{\partial v_i}{\partial \tau} + [(D_{ij} + \delta_{ij}/r_i)v_i^{(0)}]u_j = [D_{ij}^2 + D_{ij}/r_i - \delta_{ij}(a^2 + 1/r_i^2)]v_j, \quad (44)$$

$$\omega \left[D_{ij}^2 + D_{ij}/r_i - \delta_{ij}(a^2 + 1/r_i^2) \right] \frac{\partial u_j}{\partial \tau} + \frac{a^2 \eta}{(1-\eta)} \text{Ta} \frac{v_i^{(0)}}{r_i} \delta_{ij} v_j = \left[D_{ij}^4 + 2D_{ij}^3/r_i - (3/r_i^2 + 2a^2)D_{ij}^2 + (3/r_i^3 - 2a^2/r_i)D_{ij} - (3/r_i^4 - 2a^2/r_i^2 - a^4)\delta_{ij} \right] u_j, \quad (45)$$

$$\omega \frac{\partial T_{Li}}{\partial \tau} + \frac{\partial T_{Li}^{(0)}}{\partial r} \delta_{ij} u_j = \frac{1}{\text{Pr}} \left(D_{ij}^2 + D_{ij}/r_i - \delta_{ij} a^2 \right) T_{Lj}; \quad (46)$$

and in the solid, we have

$$\omega \frac{\partial T_{Si}}{\partial \tau} = \frac{1}{\text{Ps}} \left(\hat{D}_{ij}^2 + \hat{D}_{ij}/r_i - \delta_{ij} a^2 \right) T_{Sj}.$$

Here δ_{ij} is the Kronecker delta, and we sum over the repeated index j .

In both phases, the subscript 0 indicates the rigid boundary and the subscript n indicates the interface. We also have a differential equation for the interface amplitude given by

$$\omega \mathcal{L} \frac{\partial h}{\partial \tau} = -D_{nj} T_{Lj} + q \hat{D}_{nj} T_{Sj}. \quad (47)$$

Instead of satisfying the differential equation for u at x_1 and x_{n-1} , we apply the algebraic conditions

$$D_{1j} u_j = 0 \text{ and } D_{nj} u_j = 0. \quad (48)$$

The boundary condition on the azimuthal velocity becomes the algebraic equation

$$v_n^{(1)} + \left(D_{nj} v_j^{(0)} - \frac{1}{r_1} \cos \tau \right) h^{(1)} = 0. \quad (49)$$

From continuity of the temperature field at the interface we have the final two algebraic conditions

$$T_{Ln}^{(1)} + \left(\frac{\partial T_{Ln}^{(0)}}{\partial r} + \gamma a^2 - 1/r_1^2 \right) h^{(1)} = 0, \quad (50)$$

and

$$T_{Sn}^{(1)} + \left(\frac{\partial T_{Sn}^{(0)}}{\partial r} + \gamma a^2 - 1/r_1^2 \right) h^{(1)} = 0. \quad (51)$$

There are then $4n - 5$ differential equations and 5 algebraic equations to determine the $4n$ unknowns. The computer code DASSL [36] is used to solve the differential-algebraic

system in time, in a manner similar to that described by Murray *et al.*[34]. The Floquet analysis is performed by writing the solution vector F in the form

$$F(r, t) = f(r, t)e^{\sigma t},$$

where the amplitude $f(r, t)$ is periodic in time, and the complex growth rate σ determines the linear stability of the system. The numerical determination of σ is implemented by constructing the $K \times K$ fundamental solution matrix, where $K = 4n - 5$ is the number of differential equations. The eigenvalues of this matrix are the Floquet multipliers from which σ is obtained.

4.2. Narrow Gap

We also solve the narrow gap problem by using a pseudospectral discretization in the spatial variables, and this reduces the problem to ordinary differential equations in time coupled to algebraic conditions at the boundary. The discretized equations for the velocity components become

$$\omega \left(D_{ij}^2 - a^2 \delta_{ij} \right) \frac{\partial u_j}{\partial \tau} = \left(D_{ij}^4 - 2a^2 D_{ij}^2 + a^4 \delta_{ij} \right) u_j - a^2 \text{Tav}_i^{(0)} \delta_{ij} v_j, \quad (52)$$

$$\omega \frac{\partial v_i}{\partial \tau} = \left(D_{ij}^2 - \delta_{ij} a^2 \right) v_j - D_{ik} v_k^{(0)} \delta_{ij} u_j, \quad (53)$$

The equation for the temperature in the melt becomes

$$\omega \frac{\partial T_{Li}^{(1)}}{\partial \tau} = \frac{1}{\text{Pr}} \left(D_{ij}^2 - a^2 \delta_{ij} \right) T_{Lj}^{(1)} - u_i, \quad (54)$$

and in the solid,

$$\omega \frac{\partial T_{Si}^{(1)}}{\partial \tau} = \frac{1}{\text{Ps}} \left[\frac{4}{x_0^2} D_{ij}^2 - a^2 \delta_{ij} \right] T_{Sj}^{(1)}. \quad (55)$$

In both phases, the subscript 0 indicates the rigid boundary and the subscript n indicates the interface. The final differential equation determines the interface location

$$\mathcal{L} \omega \frac{\partial h^{(1)}}{\partial \tau} + D_{nj} T_{Lj}^{(1)} - q \frac{2}{x_0} D_{nj} T_{Sj}^{(1)} = 0. \quad (56)$$

Instead of satisfying the differential equation for u at x_1 and x_{n-1} , we apply the algebraic conditions

$$D_{1j}u_j = 0 \text{ and } D_{nj}u_j = 0. \tag{57}$$

The boundary condition on the azimuthal velocity becomes the algebraic equation

$$v_n^{(1)} + D_{nj}v_j^{(0)}h^{(1)} = 0. \tag{58}$$

From continuity of the temperature field at the interface we have the final two algebraic equations

$$T_{Ln}^{(1)} + h^{(1)} = T_{Sn}^{(1)} + q^{-1}h^{(1)} = -\gamma a^2 h^{(1)}. \tag{59}$$

We again have $4n - 5$ coupled differential equations and 5 algebraic conditions to determine the $4n$ unknowns.

5. Numerical Results

First, convergence of the results for the wide gap model to those for the narrow gap

Wide Gap	
η	Ta
0.69	991.23
0.9469	901.26
0.9832	899.02
0.9917	897.06

Table 1: Linear theory results verifying convergence of wide and narrow gap codes for $\omega = 28.9$ and $a = 1.866$. Note that the result in the first row is in very good agreement with previous results[25]; there, $Ta = 991.21$ for the same parameters except $\gamma = 0$. The narrow gap result ($\eta = 1$) is $Ta = 895.07$. Here the crystal width is fixed at $r_1 - r_0 = 1.33$ and $\eta_S = \eta - (r_1 - r_0)(1 - \eta)$.

model can be demonstrated, as is illustrated in Table 1.

Neutral curves for several values of the Prandtl number for the wide gap model are shown in Figure 3. For small Prandtl numbers, the neutral curve approaches that of

the rigid-walled case, while for increasing Pr , we see a destabilization of the purely hydrodynamic mode and an accompanying decrease in the critical wave number. The critical Taylor number becomes approximately proportional to Pr^{-1} as is shown in Figure 4 and Table 2. As the Prandtl number increases through unity, the neutral curve rapidly approaches the limiting shape denoted by $Pr = \infty$. This limiting neutral curve is the result of an asymptotic analysis for large Prandtl number which is discussed in the following section.

The destabilization of the centrifugal instability occurs precipitously as the Prandtl number is increased. This destabilization is apparently caused by the strong coupling of the temperature field with the flow in the melt and the subsequent transport of heat from the interface. When $Pr \gg 1$, the dominant mode of heat transfer is from convection, and the temperature field is strongly affected by the disturbance flow. For $Pr \ll 1$, heat transfer is dominated by conduction, and the flow disturbance discussed here has little effect on the interface shape[22].

Examination of the Fourier coefficients of the unstable modes shows that the response is such that the azimuthal velocity consists of only odd temporal harmonics and the remaining dependent variables consist of only even temporal harmonics; this type of response was termed "Type I" in [25], where modes having a different symmetry were also obtained in the rigid-walled system. It may further be seen that the solutions are dominated by the mean (time independent) and fundamental components (the lowest frequency terms from the Type I solutions).

6. Asymptotic theory for $Pr \gg 1$

We next describe an asymptotic analysis in the limit $Pr \rightarrow \infty$ for the destabilization of the centrifugal instability in the two-phase system. We describe the narrow gap results in detail for ease of discussion, and simply report the results for the wide gap case.

6.1. Narrow Gap

If the Prandtl number is large enough, limiting behavior occurs in the solutions to the linear problem. Some numerical results for several values of the Prandtl number with all other parameter values fixed are given in Table 2. The other parameters are fixed at values appropriate for the experiments with SCN. We note that the simpler problem with steady rotation was also amenable to large Prandtl number asymptotics [22]. We

Pr = Ps	Ta	$\mathcal{T} = \text{PrTa}$
1.0	17315.	17315.
22.8	899.79	20515.
100.	206.44	20644.
1000.	20.678	20678.

Table 2: Results of Floquet theory with pseudospectral spatial discretization for the narrow gap limit for increasing Pr number. For all of the values in the table, $\omega = 28.9$, $a = 1.75$, $\gamma = 6.2 \times 10^{-6}$, $\mathcal{L} = 409$, and $q = 1.009$. Note that the product PrTa tends to a constant as the Prandtl number increases.

now carry out an asymptotic analysis for the modulated problem in the large Prandtl number limit.

One approach to use at this point is Floquet theory with Fourier analysis, as discussed in [25]. This is suggested by an examination of the equations, with due regard to the occurrence of harmonics. As in Hall *et al.*[26, 27], one expects the Fourier coefficients to depend on Pr. The Fourier decomposition approach shows, and it is confirmed by examination of the numerically-determined Fourier coefficients of the pseudospectral solution, that the following expansions should be used:

$$v^{(1)} \sim \left[\bar{v}_1(x)e^{i\tau} + \frac{\bar{v}_3(x)}{\text{Pr}}e^{3i\tau} + \dots + c.c. \right], \tag{60}$$

$$u^{(1)} \sim \frac{1}{\text{Pr}} \left\{ \bar{u}_0(x) + \left[\bar{u}_2(x)e^{2i\tau} + \frac{\bar{u}_4(x)}{\text{Pr}}e^{4i\tau} + \dots + c.c. \right] \right\}, \tag{61}$$

$$T_L^{(1)} \sim \bar{T}_0(x) + \left[\frac{\bar{T}_2(x)}{\text{Pr}}e^{2i\tau} + \dots + c.c. \right], \tag{62}$$

$$T_S^{(1)} \sim \bar{T}_{S0}(x) + \left[\frac{\bar{T}_{S2}(x)}{\text{Pr}} e^{2i\tau} + \dots + c.c. \right], \quad (63)$$

$$\bar{h} \sim \bar{h}_0 + \left[\frac{\bar{h}_2}{\text{Pr}} e^{2i\tau} + \dots + c.c. \right], \quad (64)$$

and that the Taylor number should be scaled as $\text{Ta} = T/\text{Pr}$. Here we have assumed scalings for the first harmonics of the temperature in the solid and the interface suggested by the interfacial temperature condition; we defer to the appendix further discussion of the scaling behavior.

The problem for the mean and fundamental coefficients becomes

$$i\omega \bar{v}_1 = (\bar{D}^2 - a^2) \bar{v}_1, \quad (65)$$

$$(\bar{D}^2 - a^2)^2 \bar{u}_0 = \frac{1}{2} a^2 T (V_0 \bar{v}_1^* + c.c.), \quad (66)$$

$$\bar{u}_0 = (\bar{D}^2 - a^2) \bar{T}_0, \quad (67)$$

on $0 \leq x \leq 1$ and on $x_0 \leq x \leq 1$ we have

$$(\bar{D}^2 - a^2) \bar{T}_{S0} = 0. \quad (68)$$

At the rigid boundaries all of the dependent variables are zero, and at the interface we must have

$$\bar{u}_0 = \bar{D} \bar{u}_0 = \bar{v}_1 + \frac{1}{2} \bar{D} V_0 \bar{h}_0 = 0, \quad (69)$$

$$\bar{T}_0 + \bar{h}_0 = \bar{T}_{S0} + q^{-1} \bar{h}_0 = -\gamma a^2 \bar{h}_0, \quad (70)$$

$$\bar{D} \bar{T}_0 - q \bar{D} \bar{T}_{S0} = 0. \quad (71)$$

Here $\bar{D} = \partial/\partial x$. This *time-independent* system was solved for numerically using SUPPORT [39] from the SLATEC Common Math Library [40]; this leading-order boundary value problem represents a drastic simplification from the numerical implementations of Floquet theory described earlier in this paper. The problem may also be solved analytically to obtain a complete closed form solution. However, this closed form solution is rather complicated and no advantage is gained in interpreting results. The solution can

be expressed as the sum of a complementary part, which is independent of the Taylor number, and a particular solution which is proportional to the Taylor number.

We choose to solve the complementary part of the problem in closed form, and then determine numerically the remaining particular part to determine $\mathcal{T} = \text{PrTa}$. We find

$$\bar{v}_1(x) = \frac{-DV_0(0)}{2} \frac{\sinh \sqrt{a^2 + i\omega}(1-x)}{\sinh \sqrt{a^2 + i\omega}}, \quad (72)$$

$$\bar{u}_0(x) = \mathcal{T} \tilde{u}_0(x), \quad (73)$$

$$\bar{T}_0(x) = -(1 + \gamma a^2) \frac{\sinh a(1-x)}{\sinh a} + \mathcal{T} \tilde{T}_0(x), \quad (74)$$

and

$$\bar{T}_{S0}(x) = -\left(\frac{1}{q} + \gamma a^2\right) \frac{\sinh a(x_0 - x)}{\sinh ax_0}. \quad (75)$$

For the particular solutions (denoted by a $\tilde{}$), we then have

$$(D^2 - a^2)^2 \tilde{u}_0 = \frac{1}{2} a^2 (V_0 \bar{v}_1^* + c.c.), \quad (76)$$

$$\tilde{u}_0 = (D^2 - a^2) \tilde{T}_0, \quad (77)$$

subject to

$$\tilde{u}_0(0) = D\tilde{u}_0(0) = \tilde{T}_0(0) = \tilde{u}_0(1) = D\tilde{u}_0(1) = \tilde{T}_0(1) = 0. \quad (78)$$

Once these solutions are known, we may then determine the Taylor number via Eq. (71).

In the next section we present the corresponding simplified problem for the wide gap case, and then provide a discussion of the asymptotic results for both the narrow and wide gap cases.

6.1.1. Wide Gap

We employ the same scales as in the narrow gap case to obtain equations for the wide gap case that are valid for large Pr. The problem for the mean and fundamental coefficients becomes

$$i\omega \bar{v}_1 = (DD_* - a^2) \bar{v}_1, \quad (79)$$

$$(D^2 D_*^2 - 2a^2 D D_* + a^4) \bar{u}_0 = \frac{a^2 r_1}{2} T \frac{1}{r} (V_0 \bar{v}_1^* + c.c.), \quad (80)$$

$$\frac{\partial T_L^{(0)}}{\partial r} \bar{u}_0 = (D_* D - a^2) \bar{T}_0, \quad (81)$$

on $0 \leq x \leq 1$, and on $x_0 \leq x \leq 1$ we have

$$(D_* D - a^2) \bar{T}_{S0} = 0. \quad (82)$$

At the rigid boundaries all of the variables are zero, and at the interface we must have

$$\bar{u}_0 = D \bar{u}_0 = \bar{v}_1 + \frac{1}{2} (D V_0 - 1/r_1) \bar{h}_0 = 0, \quad (83)$$

$$\bar{T}_0 + \frac{\partial T_L^{(0)}}{\partial r} \bar{h}_0 = \bar{T}_{S0} + \frac{\partial T_L^{(0)}}{\partial r} \bar{h}_0 / q = [1/r_1^2 - a^2] \gamma \bar{h}_0, \quad (84)$$

$$D \bar{T}_0 - q D \bar{T}_{S0} = 0. \quad (85)$$

Note that $\partial T_L^{(0)} / \partial r = -1/(r \ln \eta)$. This system is again solved as a boundary value problem with SUPORT; the asymptotics have eliminated the need for Floquet theory. From the standpoint of the design of the experiment, this is a big advantage, as we shall see.

Part of the wide gap problem may be solved in closed form in terms of modified Bessel functions; however, for convenience we choose to find the solutions numerically using SUPORT. We discuss the results of the asymptotic analysis in the following section.

7. Results and Discussion

Numerical results from the asymptotic approximations Eq. (65)-(68) and Eq. (69)-(71) for the narrow gap equations and from Eq. (79)-(82) and Eq. (83)-(85) for the wide gap equations are displayed as curves labeled "Pr = ∞ " in Figures 4 and 5. These results are for a fixed frequency of $\omega = 28.9$. The neutral curves from the full Floquet theory rapidly approach these limiting results for Pr > 1, particularly for smaller wavenumbers in the neutral curve. The entire neutral curve from the asymptotic analysis can be obtained in two orders of magnitude less processing time than that required to compute a single data

point by using the full Floquet theory implementation. The limiting behavior where critical wavenumber is decreased and the Taylor number scales like the inverse of the Prandtl number [25] occurs even as the Prandtl number is near unity, and it is a good approximation to the experimental case of $Pr = 22.8$ for SCN.

Figure 5 displays the limiting behavior for the narrow gap approximation. The smaller wavenumber side of the curve is virtually unaffected by the Prandtl number variation, and as the Prandtl number increases, the higher wavenumber side approaches the asymptotic limit ($Pr = \infty$).

The wide gap and narrow gap results are compared in Figure 6; the results become insensitive to the gap width once η is larger than about 0.69. As was found in the steadily-rotating case [23], the narrow gap results bound the wide gap results from below. It appears reasonable then to use the narrow gap results to design experiments in the large Pr regime.

Table 3 displays asymptotic and numerical results for the wide gap model; in this table, the critical wave number is found as a function of the frequency for each method. It is clear from the table that as long as the frequency is not too low, the asymptotic results do a good job of approximating the Floquet theory results. The numerical results are in qualitative agreement with the preliminary experimental results. For example, the wavenumber of the instability from the experiment is about 1.7 for the conditions $\omega = 28.9$, $\eta = 0.69$, and $\eta_S = 0.286$. This is in good agreement with the theoretically determined value of $a = 1.87$. The critical Taylor number from the asymptotic theory is $Ta = 987$, while the system is observed to be unstable in the preliminary experiments for this frequency at $Ta = 2038$. This instability is still much lower than the marginal theoretical value of $Ta = 93857$ at a critical wavenumber of $a = 5.059$ for the rigid-walled system in which there is no crystal-melt interface [25]; there is no experimental data available for the rigid-walled system to our knowledge.

The asymptotic results above have been found for a nondimensional frequency that is $O(1)$ with respect to the Prandtl number. We find, however, that agreement with

ω	Asymptotic		Floquet	
	a_c	PrTa	a_c	PrTa
5.0	1.449	23193.9	1.241	30442.0
7.07	1.491	15868.9	1.387	17993.5
10.0	1.557	13075.9	1.502	13880.8
15.0	1.662	13616.7	1.637	13961.4
21.0	1.765	16915.9	1.757	17110.5
28.9	1.868	22511.4	1.866	22599.6
40.0	1.969	30032.3	1.978	30001.0
50.0	2.032	35529.0	2.043	35425.6
60.0	2.078	39996.4	2.086	39854.8
70.0	2.111	43846.2	2.120	43687.9
80.0	2.137	47385.1	2.145	47220.2
90.0	2.158	50790.7	2.166	50624.5
100.0	2.175	54152.8	2.182	53985.7
110.0	2.190	57510.5	2.197	57343.7

Table 3: Results of Floquet theory and asymptotic theory for the wide gap case. In this case, the critical wave number is found to the nearest 10^{-3} for a fixed frequency. The parameters used for this table are $\mathcal{L} = q = 1.0$, $\text{Pr} = \text{Ps} = 22.8$, $\gamma = 0$, $\eta = 0.69$, $\eta_S = 0.286$.

high frequency results from the full implementation of Floquet theory is remarkably good. Table 3 and Figure 7 illustrate these results. Although the high frequency results agree rather well, the agreement in the low frequency cases is not so good. We believe that this occurs because in the high frequency limit the time-independent modes of the solution again dominate[34], in a manner similar to that just demonstrated for the high Prandtl number regime. Though we have not carried out such an analysis, the results are reminiscent of those that would occur in an averaging analysis at high frequency. In the low frequency regime, on the other hand, the temporal behavior is complicated and cannot be described by a single mode in time[34]. The computation at the lowest frequencies is difficult for the pseudospectral approach with Floquet theory, and the computations are best performed there with the Fourier approach of [25].

Although the Floquet theory and asymptotic approximations agree closely, preliminary experimental results are only in qualitative agreement with either theory. The instability has been observed only above the neutral curves given by either theory (see Figure 4 in [25]). The effect of the deformable crystal-melt interface is pronounced; both the theoretical and experimental results show that the two-phase system is significantly less stable than the rigid-walled system.

8. Conclusion

We have modeled the destabilization of the purely azimuthal base flow in the Taylor-Couette geometry with a crystalline inner cylinder under pure torsional modulation. We have developed a pseudospectral discretization in the spatial variables and found the eigenvalues of the fundamental solution matrix of the resulting differential/algebraic system in order to determine stability or instability[34].

In addition, we have been able to carry out asymptotic analyses in the limiting case of large Prandtl number in the Taylor-Couette geometry with a crystalline inner cylinder under pure torsional modulation. In an analysis similar to the work of Hall *et al.*[26, 27] we have carried out a Fourier analysis with the amplitude of each mode depending on

the large parameter, in this case the Prandtl number. Because the leading-order mode is primarily time-independent, the "full" numerical analysis of the problem involving Floquet theory is simplified to a single boundary value problem at leading order. This results in a great reduction in computational effort. Because the coefficients of the higher-order modes also display boundary-layer structure in space (see appendix), they appear to be even smaller than the expected scalings; this helps make the analysis a particularly effective approximation. The approximation remains good in the high-frequency regime where a time-independent (or steady-streaming) mode of the solution components is dominant.

Given the preliminary nature of the experiments performed with succinonitrile, the agreement in the onset of the instability seems good. The wavenumber is reasonably approximated by the linear theory value. It appears that in the large Prandtl number regime, the transport of heat is strongly affected by the disturbance flow of the melt and that the flow in the melt is destabilized by the deformable interface. More extensive experiments would serve to clarify the correspondence between the experimental and theoretical results.

The general question of predicting whether a given hydrodynamic instability will be strongly modified if a rigid boundary is replaced by a deformable crystal-melt interface is still poorly understood. Several studies have shown that instabilities associated with critical layers in the interior of the fluid are not affected strongly by the presence of the crystal-melt interface. This is not unexpected, since for these instabilities the perturbations to the flow are generally confined to the immediate vicinity of the critical layer, and influence of the boundary conditions of the perturbed flow is not large. Examples of this type include the instabilities associated with Poiseuille flow [20], the asymptotic suction profile [16], and the buoyant instability of the parallel flow inside a vertical annulus with lateral heating [21, 20].

For instabilities of a less local nature, for which the relevant length scale of the instability is the container width, the possibility of flow/interface interaction is correspondingly

greater. Examples of this type include the shear instability of the parallel flow inside a vertical annulus with lateral heating [21, 20], Rayleigh-Bénard convection [17], steady Taylor-Couette flow [22, 23], and the modulated Taylor-Couette flow considered here. For these flows, strong couplings are observed for large Prandtl numbers, except in the case of Rayleigh-Bénard convection, where the modification of the linear stability of the system is not found to be large [17]. A common feature of the instabilities which are strongly affected by the crystal-melt interface is the presence of shear in the base state. With shear, the linearized no-slip boundary condition for the perturbed velocity produces a direct coupling between the tangential perturbation velocity and the interface deformation; this coupling is absent for a quiescent base state, as in Rayleigh-Bénard convection.

Acknowledgements

The authors are grateful for discussions with A. A. Wheeler. This work was conducted with the support of the Microgravity Science and Applications Program of NASA. One of the authors (R.J.B.) was also supported by a National Research Council Postdoctoral Fellowship.

Appendix A. Higher Order Modes

We now discuss why the lowest-order terms dominate for $Pr = Ps \gg 1$ by examining the problem for the next-order nonzero harmonics. As mentioned previously, the scalings for the harmonics is assumed from the form of the boundary conditions. From the numerical results, however, it can be seen that the scales for the coefficients of the harmonics for the interface position and the solid temperature field are of higher order than expected.

The problem for the next-order harmonic Fourier coefficients is

$$3i\omega\bar{v}_3 = (D^2 - a^2)\bar{v}_3 - \frac{1}{2}(DV_0\bar{u}_2 + \frac{1}{Pr}DV_0^*\bar{u}_4), \quad (A1)$$

$$2i\omega(D^2 - a^2)\bar{u}_2 = (D^2 - a^2)^2\bar{u}_2 - \frac{1}{2}a^2\mathcal{T}(V_0\bar{v}_1 + \frac{1}{\text{Pr}}V_0^*\bar{v}_3), \quad (\text{A2})$$

$$2i\omega\bar{T}_2 + \bar{u}_2 = \frac{1}{\text{Pr}}(D^2 - a^2)\bar{T}_2, \quad (\text{A3})$$

on $0 \leq x \leq 1$ and on $x_0 \leq x \leq 1$ we have

$$2i\omega\bar{T}_{S2} - \frac{1}{\text{Pr}_S}(D^2 - a^2)\bar{T}_{S2} = 0. \quad (\text{A4})$$

At the rigid boundaries similar homogeneous conditions hold, and at the interface we have

$$\bar{u}_2 = D\bar{u}_2 = \bar{v}_3 + \frac{1}{2}DV_0\bar{h}_2 + \frac{1}{2\text{Pr}}DV_0^*\bar{h}_4 = 0, \quad (\text{A5})$$

$$\bar{T}_2 + \bar{h}_2 = \bar{T}_{S2} + g_S\bar{h}_2 = -\gamma a^2\bar{h}_2, \quad (\text{A6})$$

$$2i\omega\mathcal{L}\bar{h}_2 + D\bar{T}_2 - qD\bar{T}_{S2} = 0. \quad (\text{A7})$$

Here the asterisk denotes complex conjugation. In order to write these equations we have assumed that the first harmonic coefficient for the interface shape and the temperature in the solid scale like $1/\text{Pr}$; this is suggested by the interfacial temperature conditions. Now to leading order for $\text{Pr} \gg 1$ in these Fourier coefficients some of the terms in the equations drop out. In particular, the heat equation in the melt yields

$$\bar{T}_2 = \frac{-1}{2i\omega}\bar{u}_2; \quad (\text{A8})$$

since $\bar{u}_2 = D\bar{u}_2 = 0$ at both the rigid wall and the interface, then $\bar{T}_2 = D\bar{T}_2 = 0$ there as well. There will be an $O(1/\text{Pr})$ correction to \bar{T}_2 . The heat equation in the solid yields that $\bar{T}_{S2} = 0$. The interfacial temperature conditions then imply that $\bar{h}_2 = 0$ to leading order. Because $D\bar{T}_2 = 0$, the heat flux at the interface vanishes to leading order as well. The Fourier coefficients for the leading order temperature in the solid \bar{T}_{S2} appears to be zero by a similar process. The velocity components \bar{u}_2 and \bar{v}_3 must come from the numerical solution of the coupled boundary value problem given by Eq. (A1)-(A4) with boundary conditions Eq. (A5)-(A7).

The problem for the correction to the leading-order Fourier coefficients may be written

down; for the next-order coefficients, let

$$\bar{u}_2 \sim \bar{u}_2^{(0)} + \frac{1}{\text{Pr}} \bar{u}_2^{(1)}, \quad (\text{A9})$$

and similarly for the other variables. Substitution into Eq. (A4) results in

$$3i\omega \bar{v}_3^{(1)} = (D^2 - a^2) \bar{v}_3^{(1)} - \frac{1}{2} (DV_0 \bar{u}_2^{(1)} + DV_0^* \bar{u}_4^{(0)}), \quad (\text{A10})$$

$$2i\omega (D^2 - a^2) \bar{u}_2^{(1)} = (D^2 - a^2)^2 \bar{u}_2^{(1)} - a^2 \mathcal{T} \frac{1}{2} (V_0 \bar{v}_1^{(1)} + V_0^* \bar{v}_3^{(0)}), \quad (\text{A11})$$

$$2i\omega \bar{T}_2^{(1)} + \bar{u}_2^{(1)} = (D^2 - a^2) \bar{T}_2^{(0)}, \quad (\text{A12})$$

on $0 \leq x \leq 1$ and on $x_0 \leq x \leq 1$ we have

$$2i\omega \bar{T}_{S_2}^{(1)} - \frac{1}{\text{Pr}} (D^2 - a^2) \bar{T}_{S_2}^{(0)} = 0. \quad (\text{A13})$$

At the rigid boundaries all of the variables are zero, and at the interface we must have

$$\bar{u}_2^{(1)} = D\bar{u}_2^{(1)} = \bar{v}_3^{(1)} + DV_0 \bar{h}_2^{(1)} + DV_0^* \bar{h}_4^{(0)} = 0, \quad (\text{A14})$$

$$\bar{T}_2^{(1)} + \bar{h}_2^{(1)} = \bar{T}_{S_2}^{(1)} + g_S \bar{h}_2^{(1)} = -\gamma a^2 \bar{h}_2^{(1)}, \quad (\text{A15})$$

$$2i\omega \mathcal{L} \bar{h}_2^{(1)} + D\bar{T}_2^{(1)} - qD\bar{T}_{S_2}^{(1)} = 0. \quad (\text{A16})$$

The term $\bar{h}_4^{(0)}$ is identically zero; this is shown by a similar procedure to that for $\bar{h}_2^{(0)}$. It appears from this problem that the interfacial temperature coefficient $\bar{T}_2^{(1)}$ will be nonzero at the interface and numerical results show that the $\bar{h}_2 = O(\text{Pr}^{-2})$ and thus that $\bar{h}_2^{(1)} \neq 0$. These two observations suggest that there is a boundary layer of width $\text{Pr}^{1/2}$ in the coefficient for the solid temperature coefficient $\bar{T}_{S_2}^{(1)}$. If we rescale that equation with $x = \text{Pr}^{1/2} \hat{x}$ the equation for the inner part of the solid temperature coefficient is

$$2i\omega \hat{T}_{S_2}^{(1)} - \hat{D}^2 \hat{T}_{S_2}^{(1)} = 0, \quad (\text{A17})$$

which has a solution of the form

$$\bar{T}_{S_2}^{(1)} = C_1 \exp[(1-i)\sqrt{\omega}x/\text{Pr}^{1/2}]. \quad (\text{A18})$$

There is no boundary layer at the rigid wall, and this inner solution matches automatically with the trivial interior solution. The rest of the solution at this order can be

found though the solution may no longer be found sequentially. This boundary layer is compatible with $\bar{T}_2^{(1)} \neq 0$ and $\bar{h}_2^{(1)} \neq 0$.

We believe that the small or non-existent numerical amplitudes of the higher harmonic modes contributes to the success of the asymptotic approximation.

References

- [1] D. T. J. Hurle, "Convective transport in melt growth systems," *J. Crystal Growth* **65** (1983) pp. 124-132.
- [2] R. A. Brown, "Theory of transport processes in single crystal growth from the melt," *AIChE J.* **34** (1988) pp. 881-911.
- [3] D. T. J. Hurle and E. Jakeman, "Introduction to the techniques of crystal growth," *PCH PhysicoChem. Hydrodyn.* **2** (1981) pp. 237-244.
- [4] W. W. Mullins and R. F. Sekerka, "Stability of a planar interface during solidification of a dilute binary alloy," *J. Appl. Phys.* **35** (1964) pp. 444-451.
- [5] S. R. Coriell, G. B. McFadden and R. F. Sekerka, "Cellular growth during directional solidification," *Ann. Rev. Mater. Sci.* **15** (1985) pp. 119-145.
- [6] M. E. Glicksman, S. R. Coriell and G. B. McFadden, "Interaction of flows with the crystal-melt interface," *Annu. Rev. Fluid Mech.* **18** (1986) pp. 307-335.
- [7] S. R. Coriell and R. F. Sekerka, "Effect of convective flow on morphological stability," *PCH PhysicoChem. Hydrodyn.* **2** (1981) pp. 281-293.
- [8] S. H. Davis, "Hydrodynamic interactions in directional solidification," *J. Fluid. Mech.* **212** (1990) pp. 241-262.
- [9] R. T. Delves, "Theory of Interface Stability," in *Crystal Growth*, B. R. Pamplin, ed. (Pergamon, Oxford, 1974) pp. 40-103.

- [10] S. R. Coriell, G. B. McFadden, R. F. Boisvert, and R. F. Sekerka, "Effect of a forced Couette flow on coupled convective and morphological instabilities during unidirectional solidification," *J. Crystal Growth* **69** (1984) pp. 15-22.
- [11] S. R. Coriell, M. R. Cordes, W. J. Boettinger, and R. F. Sekerka, "Convective and interfacial instabilities during unidirectional solidification of a binary alloy," *J. Crystal Growth* **49** (1980) pp. 13-28.
- [12] S. R. Coriell and G. B. McFadden, "Buoyancy effects on morphological instability during directional solidification," *J. Crystal Growth* **94** (1989) pp. 513-521.
- [13] K. Brattkus, and S. H. Davis, "Flow induced morphological instability: stagnation point flows," *J. Crystal Growth* **89** (1988) pp. 423-427.
- [14] G. B. McFadden, S. R. Coriell, and J. I. D. Alexander, "Hydrodynamic and free boundary instabilities during crystal growth: the effect of a plane stagnation flow," *Comm. Pure and Appl. Math* **41** (1988) pp. 683-706.
- [15] K. Brattkus and S. H. Davis, "Flow induced morphological instability: the rotating disk," *J. Crystal Growth* **87** (1988) pp. 385-396.
- [16] S. A. Forth and A. A. Wheeler, "Hydrodynamic and morphological stability of the unidirectional solidification of a freezing binary alloy: a simple model," *J. Fluid Mech.* **202** (1989) pp. 339-366.
- [17] S. H. Davis, U. Müller, and C. Dietsche, "Pattern selection in single-component systems coupling Bénard convection and solidification," *J. Fluid. Mech.* **144** (1984) pp. 133-151.
- [18] B. Caroli, C. Caroli, C. Misbah, and B. Roulet, "Solutal convection and morphological instability in directional solidification of binary alloys," *J. Phys. (Paris)* **46** (1985) pp. 401-413.

- [19] G. W. Young and S. H. Davis, "Directional solidification with buoyancy in systems with small segregation coefficient," *Phys. Rev.* **B34** (1986) pp. 3388-3396.
- [20] G. B. McFadden, S. R. Coriell, R. F. Boisvert, M. E. Glicksman, and Q. T. Fang, "Morphological stability in the presence of fluid flow in the melt," *Metall. Trans.* **15A** (1984) pp. 2117-2124.
- [21] Q. T. Fang, M. E. Glicksman, S. R. Coriell, G. B. McFadden, and R. F. Boisvert, "Convective influence on the stability of a crystal-melt interface," *J. Fluid Mech.* **151** (1985) pp. 121-140.
- [22] G. B. McFadden, S. R. Coriell, M. E. Glicksman, and M. E. Selleck, "Instability of a Taylor-Couette flow interacting with a crystal-melt interface," *PCH PhysicoChem. Hydrodyn.* **11** (1989) pp. 387-409.
- [23] G. B. McFadden, S. R. Coriell, B. T. Murray, M. E. Glicksman, and M. E. Selleck, "Effect of a crystal-melt interface on Taylor-vortex flow," *Phys. Fluids A* **2** (1990) pp. 700-705.
- [24] G. I. Taylor, "Stability of a viscous liquid contained between two rotating cylinders," *Phil. Trans. Roy. Soc. A* **223** (1923) pp. 289-343.
- [25] G. B. McFadden, B. T. Murray, S. R. Coriell, M. E. Glicksman, and M. E. Selleck, "Effect of Modulated Taylor-Couette Flows on Crystal-Melt Interfaces: Theory and Initial Experiments", in *On the Evolution of Phase Boundaries*, edited by M. E. Gurtin and G. B. McFadden, IMA Series in Mathematics and Its Applications, Vol. 43 (Springer-Verlag, New York, 1992) pp. 81-100.
- [26] P. Hall, "The stability of unsteady cylinder flows," *J. Fluid Mech.* **67** (1975) pp. 29-63.
- [27] G. Seminara and P. Hall, "Centrifugal instability of a Stokes layer: linear theory," *Proc. R. Soc. Lond. A* **350** (1976) pp. 299-316.

- [28] R. C. DiPrima, "Stability of nonrotationally symmetric disturbances for viscous flow between rotating cylinders," *Phys. Fluids* **4** (1961) pp. 751-755.
- [29] P. J. Riley and R. L. Laurence, "Linear stability of modulated circular Couette flow," *J. Fluid Mech.* **75** (1976) pp. 625-646.
- [30] S. Carmi and J. I. Tustaniwskyj, "Stability of modulated finite-gap cylindrical Couette flow: linear theory," *J. Fluid Mech.* **108** (1981) pp. 19-42.
- [31] C. F. Barenghi and C. A. Jones, "Modulated Taylor-Couette flow," *J. Fluid Mech.* **208** (1989) pp. 127-160.
- [32] H. Kuhlmann, D. Roth, and M. Lucke, "Taylor vortex flow under harmonic modulation of the driving force," *Phys. Rev. A* **39** (1989) pp. 745-762.
- [33] X. Wu and J. B. Swift, "Onset of secondary flow in the modulated Taylor-Couette system," *Phys. Rev. A* **40** (1989) pp. 7192-7201.
- [34] B. T. Murray, G. B. McFadden, and S. R. Coriell, "Stabilization of Taylor-Couette flow due to time-periodic outer cylinder oscillation," *Phys. Fluids A* **2** (1990) pp. 2147-2156.
- [35] G. B. McFadden, B. T. Murray, S. R. Coriell, M. E. Glicksman, and M. E. Selleck, "Effect of a crystal-melt interface on Taylor-Vortex flow with buoyancy," *Proceedings of the 5th International Colloquium on Free Boundary Problems: Theory and Applications*, (Montreal, June 13-22, 1990).
- [36] L. R. Petzold, "A Description of DASSL: A Differential/Algebraic System Solver", SAND82-8637, (Sandia National Laboratories, Albuquerque, NM, 1982).
- [37] C. Canuto, M.Y. Hussaini, A. Quarteroni, and T.A. Zang, *Spectral Methods in Fluid Mechanics*, (Springer, New York, 1988).

-
- [38] D. Gottlieb, M.Y. Hussaini, and S.A. Orszag, in *Spectral Methods for Partial Differential Equations*, G.R. Voigt, D. Gottlieb, and M.Y. Hussaini, eds., (SIAM, Philadelphia, 1984) pp. 1-54.
- [39] M. R. Scott and H. A. Watts, "Computational solution of linear two-point boundary value problems via orthonormalization," *SIAM J. Numer. Anal.*, 14 (1977) 40-70.
- [40] SLATEC Common Math Library, Package 181-CY001-00, Energy Science and Technology Software Center, P.O. Box 1020, Oak Ridge, TN. 37381.

Figure Captions

Figure 1 Schematic diagram of the crystalline inner annulus (labeled "S") surrounded by the liquid phase (labeled "L"). In the base state the unperturbed crystal-melt interface is cylindrical, with $R_1(z', t') = \bar{R}_1$.

Figure 2 Multiple-exposure profile of the instability of a temporally-modulated crystal-melt interface, with a heated outer cylinder and a cooled inner cylinder. The material is succinonitrile with Prandtl number $Pr = 22.8$. An elongated, flexible particle circulates in the fluid and delineates the structure of the flow field in half of a Taylor vortex cell. The half-cell containing the particle is about 14 mm from crest to trough in the axial direction, corresponding to a wavenumber of about $a = 1.1$.

Figure 3 Neutral curves in the (Ta, a) -plane for several values of the Prandtl number are displayed. The other parameter values are $\omega = 28.9$, $\mathcal{L} = 409$, $q = 1.009$, $Pr = Ps = 22.8$, $\gamma = 6.2 \times 10^{-6}$, $\eta = 0.69$, $\eta_S = 0.286$. The uppermost curve ($Pr = 0.1$) approaches the rigid-walled neutral curve displayed in [25]. The base state described in Section 3.1.1 is stable below the curves and unstable above them.

Figure 4 Neutral curves in the (\mathcal{T}, a) -plane, where $\mathcal{T} = PrTa$. The parameter values are the same as for Figure 3. The case $Pr = \infty$ is the result of the asymptotic analysis described in Section 6.1.1. The base state described in Section 3.1.1 is stable below the curves and unstable above them.

Figure 5 Neutral curves in the (\mathcal{T}, a) -plane, where $\mathcal{T} = PrTa$. The parameter values are the same as for Figure 3, except that η is no longer a parameter in the problem. The case $Pr = \infty$ is the result of the asymptotic analysis described in Section 6.1. The base state described in Section 3.2.1 is stable below the curves and unstable above them.

Figure 6 Neutral curves in the (\mathcal{T}, a) -plane, where $\mathcal{T} = PrTa$, for several gap widths η . All other parameters are the same as Figure 4, and $Pr = Ps = 22.8$. The lowermost

curve is the narrow gap limit; the other curves are wide gap results.

Figure 7 Neutral curves in the (\mathcal{T}, ω) -plane, where $\mathcal{T} = \text{PrTa}$, displaying the wide gap results in Table 3. The upper curve is the result of Floquet theory data while the lower curve is the result of the asymptotic theory. The base state described in Section 3.1.1 is unstable above the curves and stable below them.

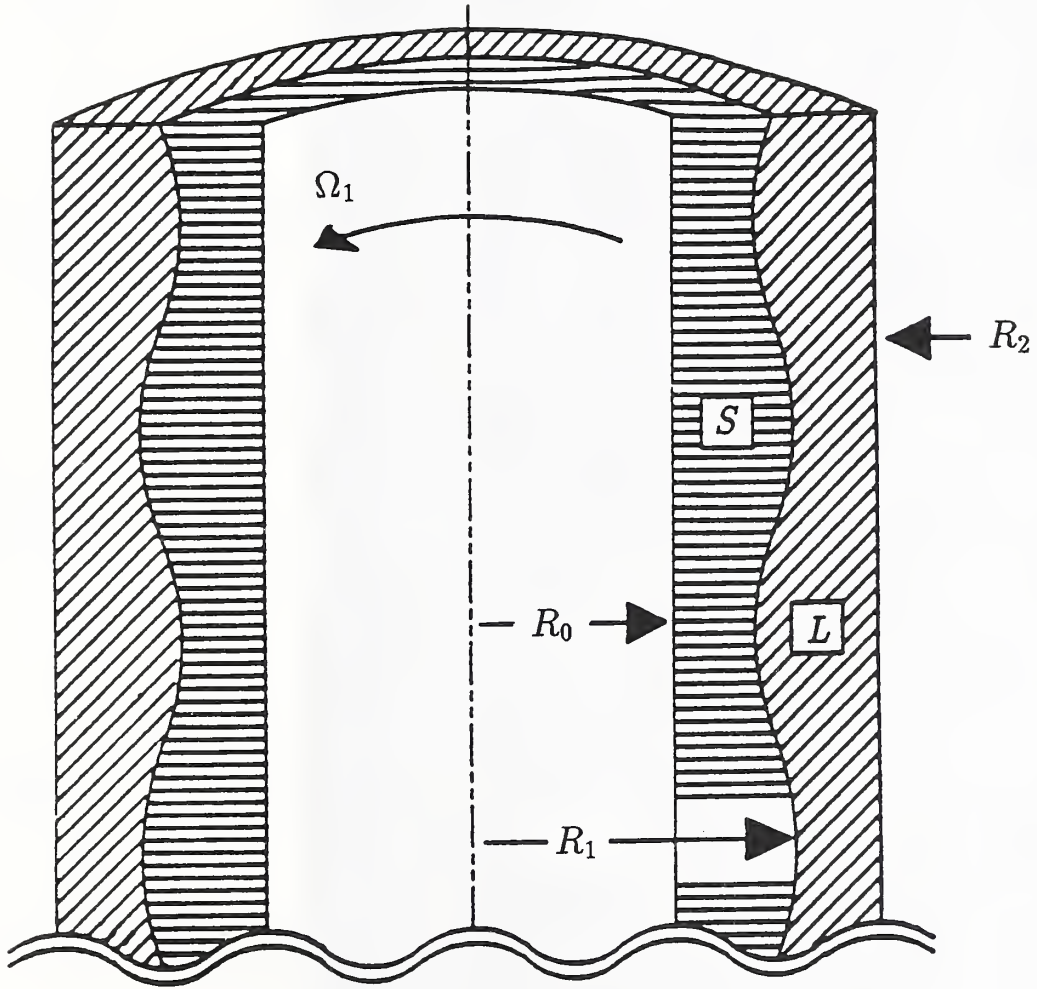


FIGURE 1

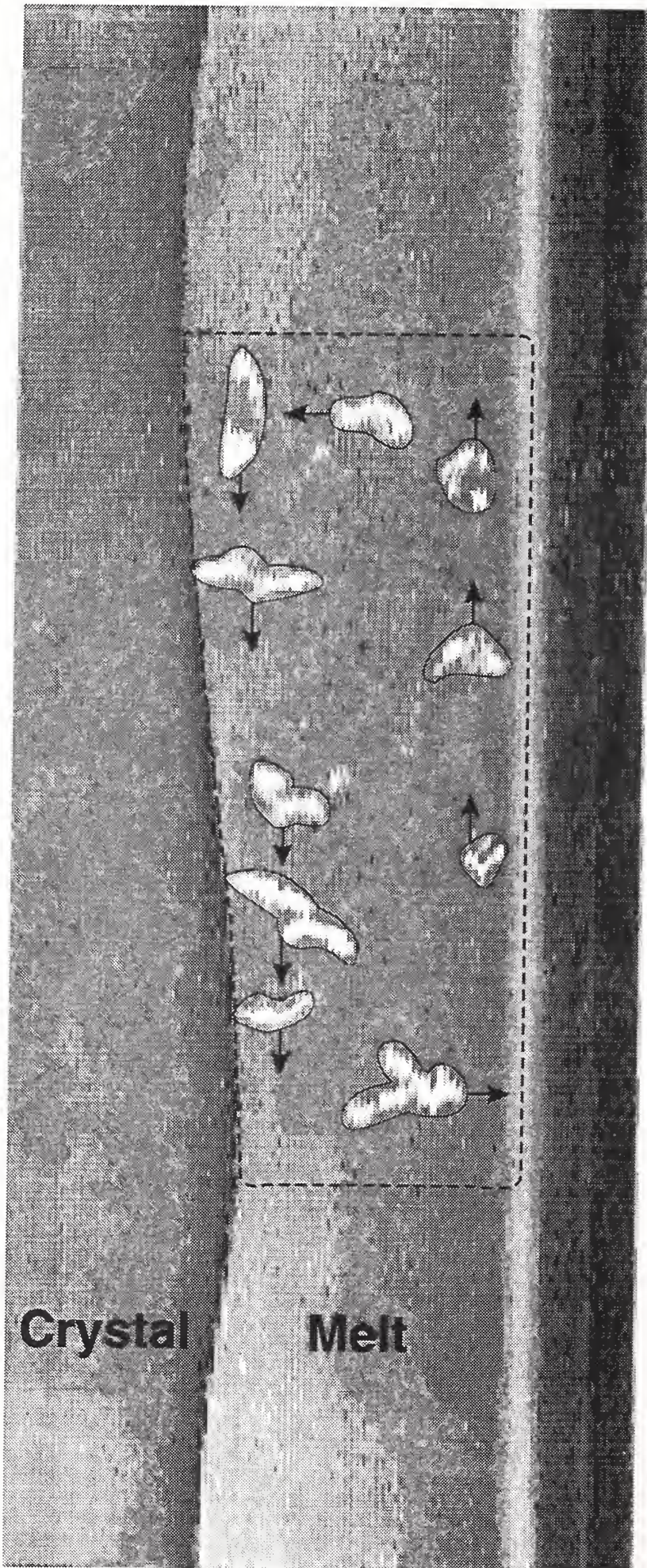


FIGURE 2

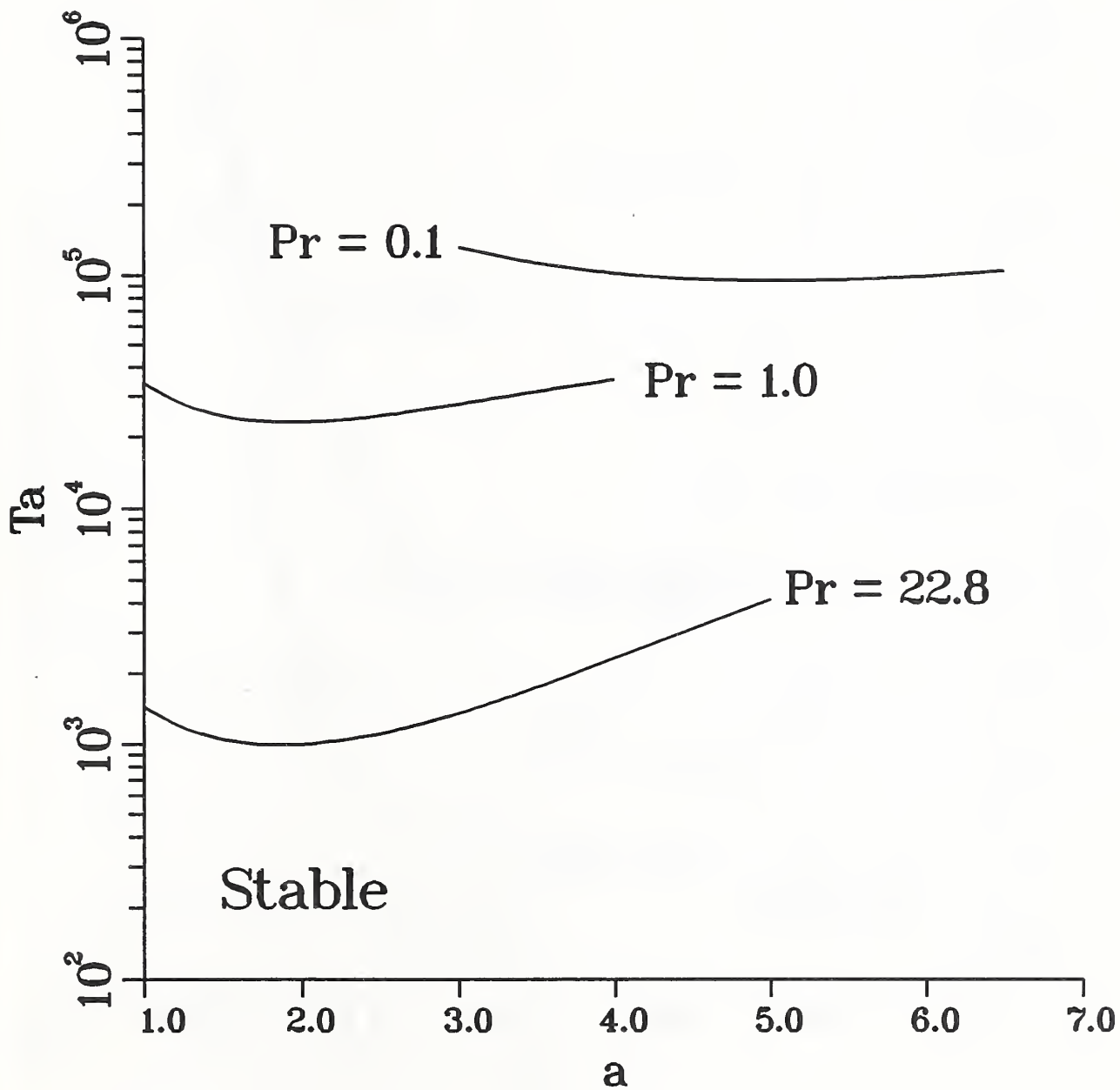


FIGURE 3

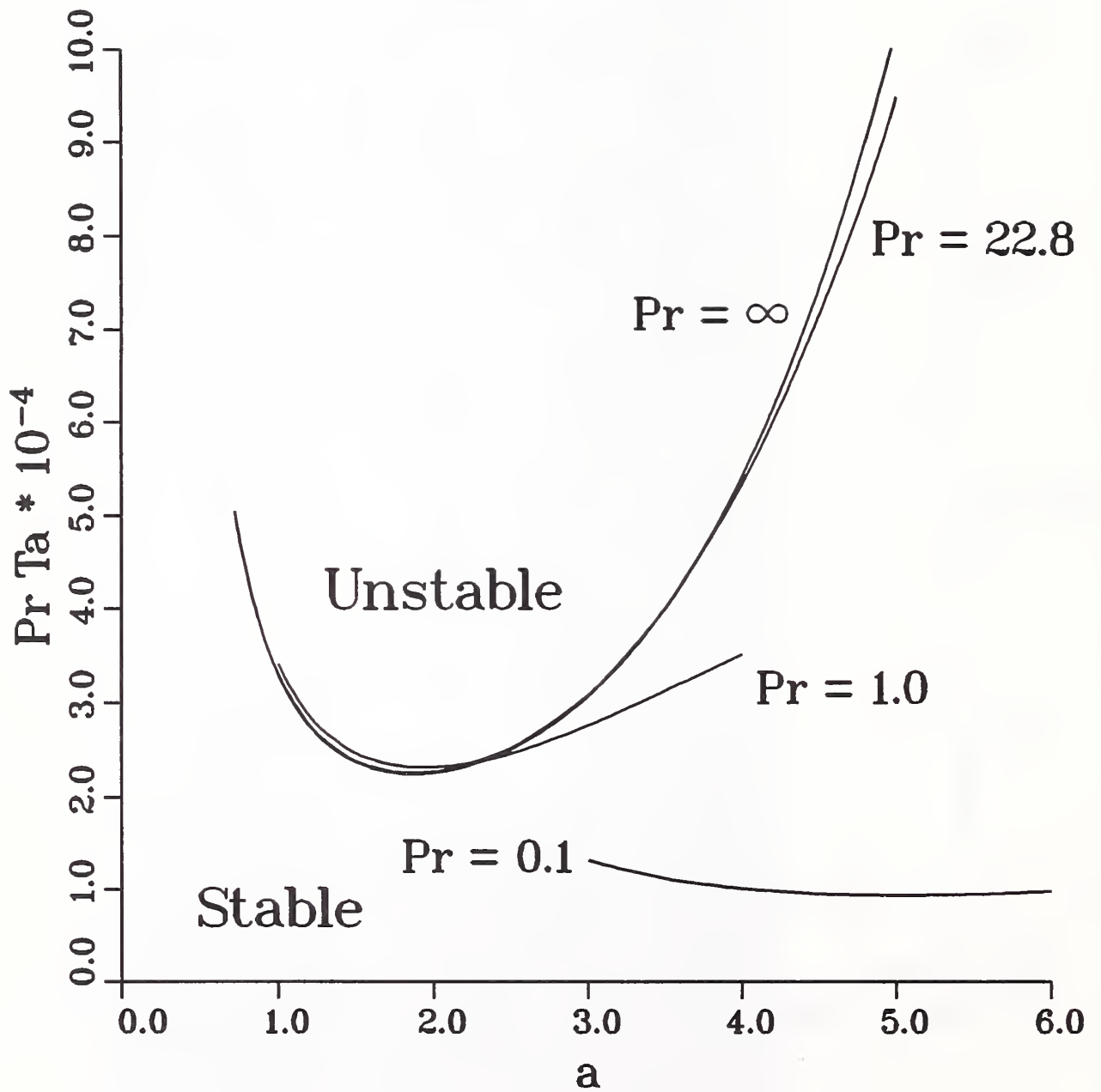


FIGURE 4

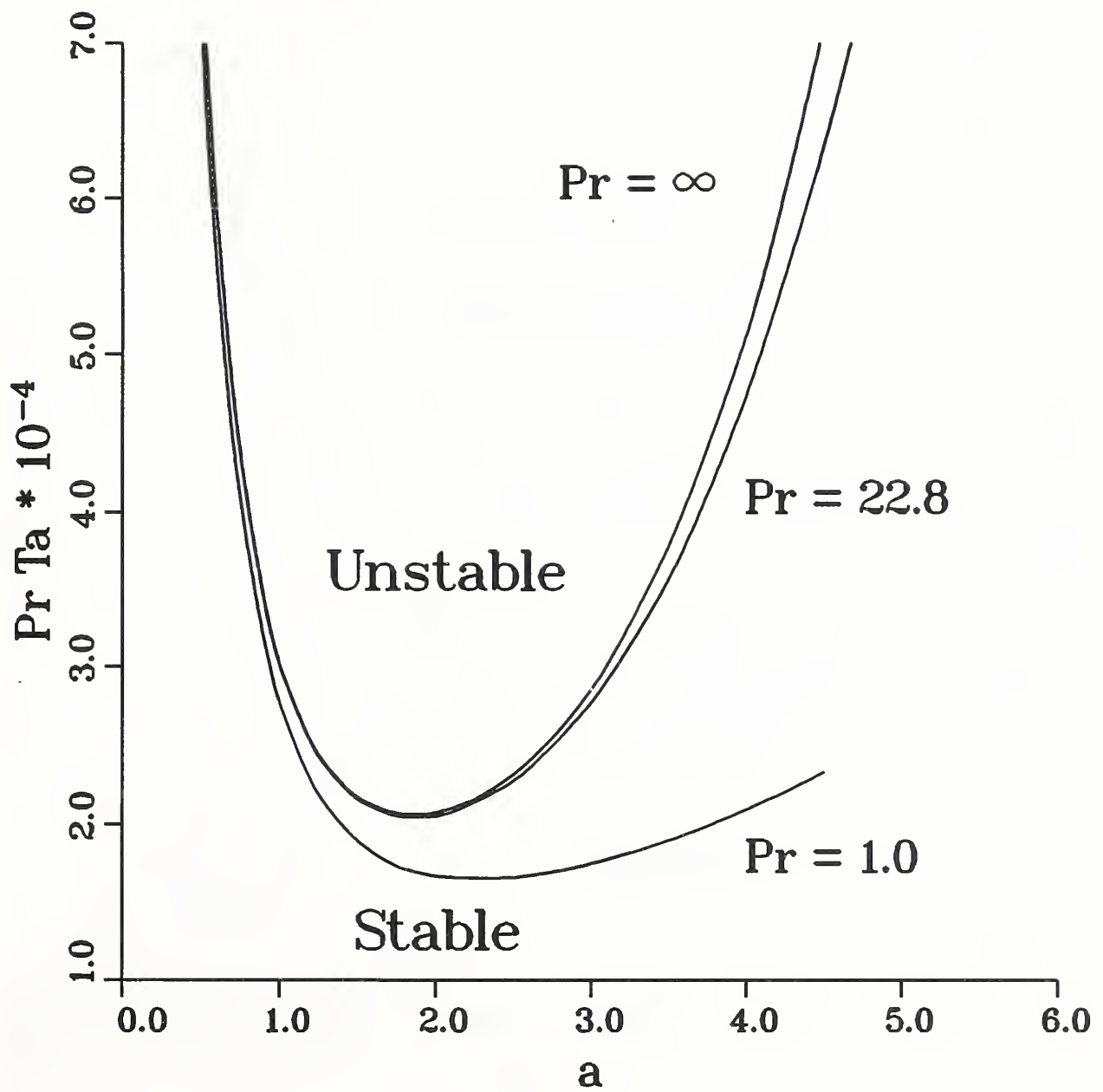


FIGURE 5

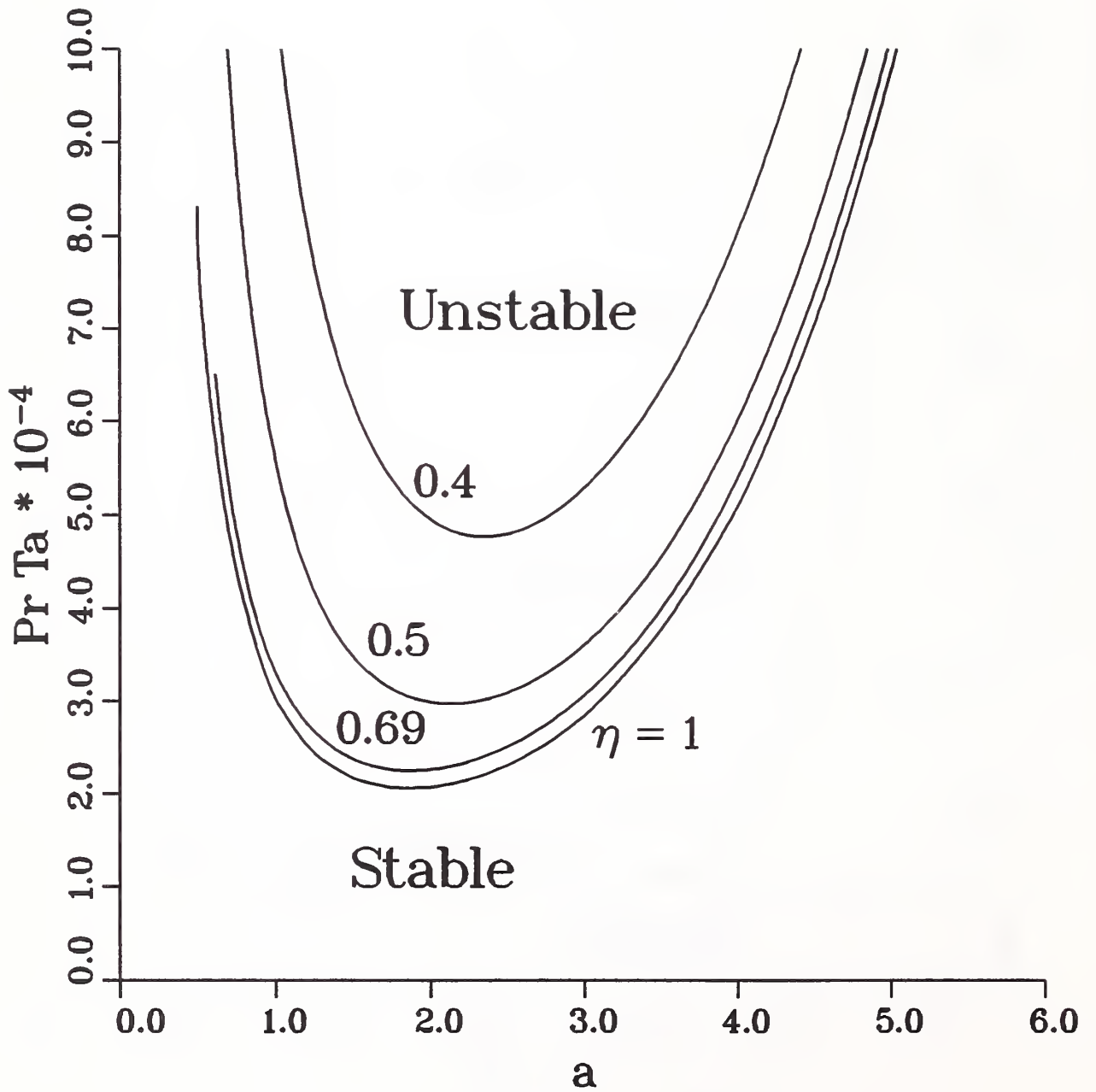


FIGURE 6

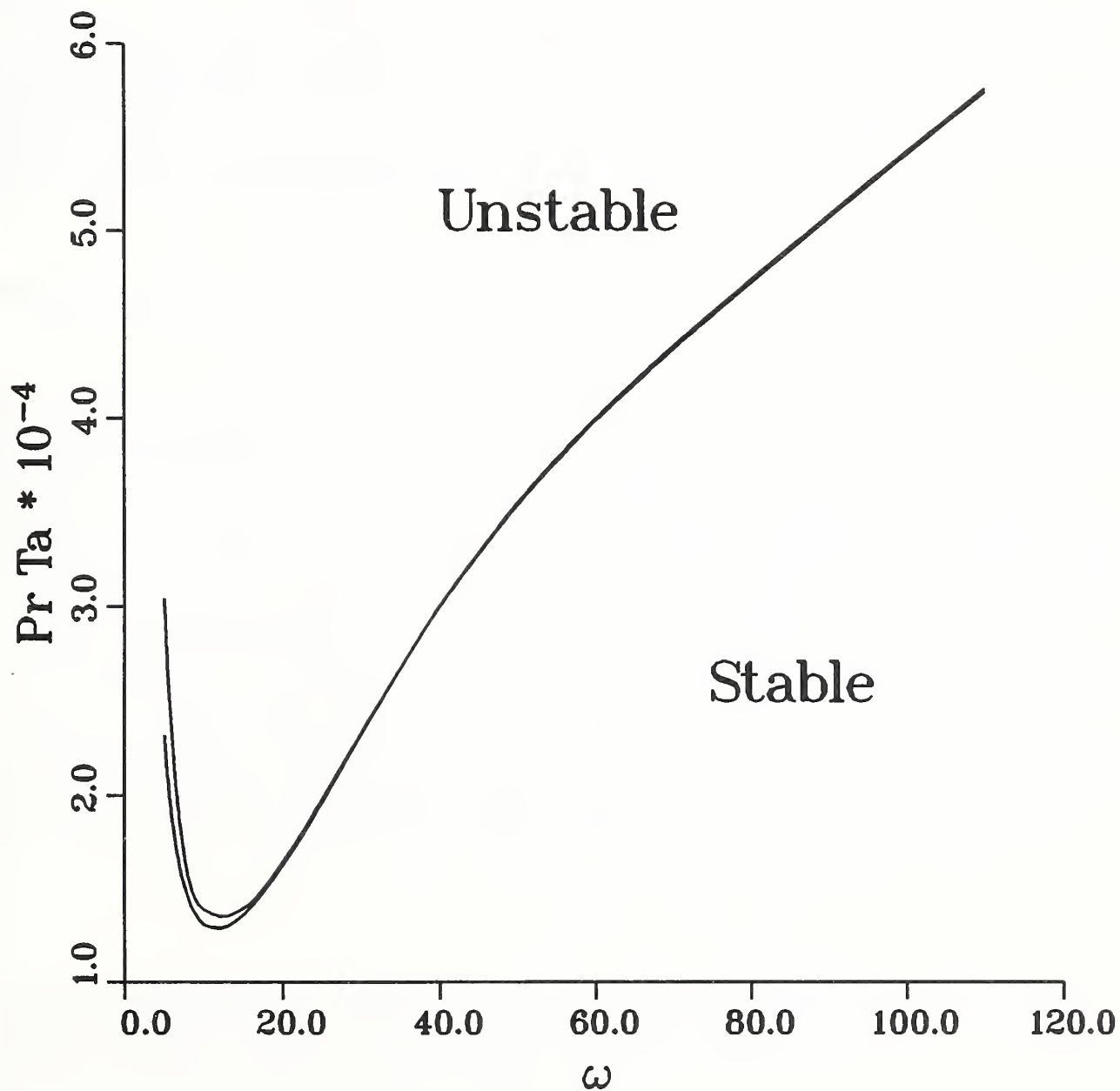


FIGURE 7

NIST-114A
(REV. 3-90)

U.S. DEPARTMENT OF COMMERCE
NATIONAL INSTITUTE OF STANDARDS AND TECHNOLOGY

BIBLIOGRAPHIC DATA SHEET

1. PUBLICATION OR REPORT NUMBER

NISTIR 4971

2. PERFORMING ORGANIZATION REPORT NUMBER

3. PUBLICATION DATE

NOVEMBER 1992

4. TITLE AND SUBTITLE

Asymptotic Behavior of Modulated Taylor-Couette Flows with a Crystalline Inner Cylinder

5. AUTHOR(S)

R.J. Braun, G.B. McFadden, B.T. Murray, S.R. Coriell, M.E. Glicksman, and M.E. Selleck

6. PERFORMING ORGANIZATION (IF JOINT OR OTHER THAN NIST, SEE INSTRUCTIONS)

U.S. DEPARTMENT OF COMMERCE
NATIONAL INSTITUTE OF STANDARDS AND TECHNOLOGY
GAITHERSBURG, MD 20899

7. CONTRACT/GRANT NUMBER

8. TYPE OF REPORT AND PERIOD COVERED

9. SPONSORING ORGANIZATION NAME AND COMPLETE ADDRESS (STREET, CITY, STATE, ZIP)

10. SUPPLEMENTARY NOTES

11. ABSTRACT (A 200-WORD OR LESS FACTUAL SUMMARY OF MOST SIGNIFICANT INFORMATION. IF DOCUMENT INCLUDES A SIGNIFICANT BIBLIOGRAPHY OR LITERATURE SURVEY, MENTION IT HERE.)

We consider the linear stability of a modulated Taylor-Couette system when the inner cylindrical boundary consists of a crystalline solid-liquid interface. Both experimentally and in numerical calculations it is found that the two-phase system is significantly less stable than the analogous rigid-walled system for materials with moderately large Prandtl numbers. A numerical treatment based on Floquet theory is described, which gives results that are in good agreement with preliminary experimental findings. In addition, this instability is further examined by carrying out a formal asymptotic expansion of the solution in the limit of large Prandtl number. In this limit the Floquet analysis is considerably simplified, and the linear stability of the modulated system can be determined to leading order through a conventional stability analysis, without recourse to Floquet theory. The resulting simplified problem is then studied for both the narrow gap geometry and for the case of a finite gap. It is surprising that the determination of the linear stability of the two-phase system is considerably simpler than that of the rigid-walled system, despite the complications introduced by the presence of the crystal-melt interface.

12. KEY WORDS (6 TO 12 ENTRIES; ALPHABETICAL ORDER; CAPITALIZE ONLY PROPER NAMES; AND SEPARATE KEY WORDS BY SEMICOLONS)

crystal-melt interface; flow-interface interaction; hydrodynamic instability; morphological instability; solidification; and Taylor-Couette flow.

13. AVAILABILITY

UNLIMITED

FOR OFFICIAL DISTRIBUTION. DO NOT RELEASE TO NATIONAL TECHNICAL INFORMATION SERVICE (NTIS).

ORDER FROM SUPERINTENDENT OF DOCUMENTS, U.S. GOVERNMENT PRINTING OFFICE,
WASHINGTON, DC 20402.

ORDER FROM NATIONAL TECHNICAL INFORMATION SERVICE (NTIS), SPRINGFIELD, VA 22161.

14. NUMBER OF PRINTED PAGES

46

15. PRICE

A03

ELECTRONIC FORM

